PHILOSOPHICAL TRANSACTIONS OF THE ROYAL SOCIETY A MATHEMATICAL, PHYSICAL & ENGINEERING SCIENCES

Rydberg states of triatomic hydrogen

C. H. Greene and J. A. Stephens

Phil. Trans. R. Soc. Lond. A 1997 **355**, 1609-1621
doi: 10.1098/rsta.1997.0079

Rydberg states of triatomic hydrogen

By C. H. Greene[1] and J. A. Stephens[2]

[1]*Department of Physics and JILA, University of Colorado, Boulder, CO 80309-0440, USA*

[2]*International Atomic Energy Agency, P.O. Box 100, A-1400 Vienna, Austria*

We describe a theoretical treatment of the Rydberg electron dynamics in triatomic hydrogen, at a level that includes the full rotational and vibrational motions of the residual ion. Preliminary results obtained very recently are also presented for triatomic deuterium.

1. Introduction

The metastability of the $\tilde{B}\ 1s^2 2p\ ^2A_2''$ state of triatomic hydrogen has led to a host of spectroscopic studies of this intriguing molecule, which apparently possesses no true bound states. Although the unstable nature of H_3 limits its potential chemical usefulness, its study provides a potent training ground for both theoretical and experimental calisthenics. The Rydberg spectroscopy of H_3 has been studied in two different regimes. The first regime involves relatively high orbital angular momenta of the Rydberg electron. For these levels it is possible to treat the electron interaction with the molecular ion as a weak perturbation. The second regime of low orbital momenta, associated with penetrating Rydberg electron orbits that sample the core non-perturbatively, requires greater sophistication in order to describe the spectrum successfully. It is the theoretical description of this second, strongly interacting class of Rydberg states of triatomic hydrogen, which forms the subject of the present study.

A great leap forward in this field was pioneered by the work of Helm and co-workers (Helm 1986; Lembo *et al.* 1989; Bordas *et al.* 1991; Bordas & Helm 1991), who formed the aforementioned metastable state in a charge exchange collision between H_3^+ and neutral Cs. The metastable trihydrogen was next stimulated to reach higher energies by a sequence of laser excitation steps. These reached bound and ionizing states near the lower ionization thresholds. Three different types of theoretical efforts had described aspects of the problem, prior to our efforts (Stephens & Greene 1994, 1995). Specifically, the physics of ℓ-uncoupling for an electron in the field of this ion with D_{3h} symmetry was unravelled by Pan & Lu (1988), without treating the vibrational motion. A crucial *ab initio* quantum chemical calculation by Nager & Jungen (1982) determined the electronic energy surfaces for clamped nuclei in a wide range of geometries.

Yet another crucial theoretical study was the work of Sobolewski & Domcke (1988), Staib *et al.* (1990) and Staib & Domcke (1990), who treated Jahn–Teller (JT) interactions in H_3 by incorporating the Longuet–Higgins Hamiltonian into a multichannel quantum defect (MQDT)-type treatment. This work was important for developing,

Phil. Trans. R. Soc. Lond. A (1997) **355**, 1609–1621
Printed in Great Britain

in essence, the tools needed to perform a vibrational frame transformation that describes Jahn–Teller effects.

The aim of the work reviewed here, which was originally published in two articles (Stephens & Greene 1994, 1995) has been to incorporate all three of these theoretical elements into a unified treatment of a Rydberg electron that moves in the field of a rotating, vibrating H_3^+ ion. This full rovibronic frame transformation treatment within an MQDT framework enables us to account semiquantitatively for a number of features observed in the experimental spectra. We also present some preliminary calculations of the photoionization of the $1s^2 3s\,^2A_2'$ Rydberg state of D_3, which can also be prepared from its metastable $\tilde{B}\ 1s^2 2p\,^2A_2''$ state. We compare the predictions to those of H_3 over a range *ca.* $1400\,\mathrm{cm}^{-1}$ above the first ionic threshold for each molecule, and discuss some expected differences between the isotopomers.

2. Frame transformation treatment

The starting point of this treatment is the realization that the exact solution can be written accurately at sufficiently large Rydberg electron distances $r > r_0$ in the 'usual' MQDT form in terms of a reaction matrix K as

$$\Psi_{i'} = Ar^{-1} \sum_{i=1}^{N_t} \Phi_i(\omega)(f_i(r)\delta_{ii'} - g_i(r)K_{ii'}). \tag{2.1}$$

Here $\Phi_i(\omega)$ represents a complete rovibronic state of the H_3^+ core, including the electronic and spin portions of its wavefunction. Each channel index $i = \{v^+ \Gamma^+ N^+ K^+\}$ includes all of the quantum numbers needed to fully characterize the core eigenstate at energy E_i, including the D_{3h} group symmetry label Γ^+. The Coulomb wavefunctions (f_i, g_i) in equation (2.1) are understood to be evaluated for the appropriate Rydberg orbital angular momentum $l = 1$, which is restricted to p-waves only in this paper as in Stephens & Greene (1994, 1995). The Coulomb functions are also understood to be evaluated at an energy for the outermost electron which is constrained by energy conservation to be $\varepsilon_i = E - E_i$. The elements of the reaction matrix characterize the scattering among open channels having $\varepsilon_i > 0$ (which we denote as $i\epsilon P$) and, among the closed channels, having $\varepsilon_i < 0$ (which we denote as $i\epsilon Q$). Multiple reflections of the Rydberg electron wavefunctions in the closed channels are responsible for all resonances that arise in our calculations, as these are all Feshbach resonances and not shape resonances. In practice, a 'reaction volume radius', r_0, and an appropriate number of channels, N_t, can be chosen such that equation (2.1) essentially involves no approximation whatsoever.

The exact *ab initio* determination of the reaction matrix K, and of a corresponding set of electric dipole amplitudes d_i, would prove to be a daunting task in general. In circumstances such as the present one, fortunately, it can be determined through a rovibronic frame transformation. This results in an enormous simplification of the computational demands in this problem. The following is an abbreviated description of the physics contained in the frame transformation appropriate to this system. For a more complete exposition, the reader is referred to Stephens & Greene (1994, 1995).

The frame transformation approximation amounts to an assumption that the Rydberg electron wavefunction changes 'suddenly' in some sense, as the electron moves from the outer region ($r > r_0$) into the inner region ($r < r_0$). This approximation

works well when two different sets of operators commute with the local Hamiltonian in the inner and outer regions and when the time involved in crossing from one region to another is short compared with the periods of all other motions. The inner operators are mutually compatible and thus their eigenstates remain 'conserved' while the electron moves within the reaction volume. Likewise the outer operators are mutually compatible with each other and remain constants of motion while the Rydberg electron moves in the purely Coulomb potential at $r > r_0$. The 'inside' operators, however, are not quantum mechanically compatible with the 'outside' operators. The operators that are diagonal for long range Rydberg electron motion include the *ionic squared angular momentum* operator $\boldsymbol{N}^{+2}$ with eigenvalues $N^+(N^+ + 1)$ and the set of *vibrational quantum numbers* $v_1 v_2^l$ for an ionic molecular state of H_3^+. This combination of quantum numbers is 'conserved' in the sense that (ignoring the weak long range multipole interactions) the electron cannot exchange energy or angular momentum with the ionic core at large distances. On the other hand, at small distances r, the Rydberg electron is moving with great speed owing to its large kinetic energy acquired from the attractive Coulomb potential. In the small-r region, accordingly, molecular body-frame quantum numbers are more applicable. When the ionic species has a definite symmetry, as in the present example where the ion possesses D_{3h} symmetry, one of the quantum numbers will be a label for a particular irreducible representation of the relevant point group symmetry. In the present example of a purely p-wave electron, the symmetry quantum number is equivalent to specification of Λ, the *projection of the orbital angular momentum* vector $\boldsymbol{L}$ onto the symmetry axis $\hat{z}$ normal to the plane containing the three nuclei. Consistent with the notions in the Born–Oppenheimer approximation, the other quantum numbers that are 'conserved' during the brief time in which the electron darts in and out of the reaction zone are the *instantaneous position vectors* of the nuclei, $\boldsymbol{Q}$.

The idea of 'suddenness' comes into the calculation through the notion that a rapid traversal of an electron through the transition region ($r \approx r_0$) simply leads to a projection of the internal eigenstates onto the external eigenstates. One factor of the projection will be

$$\langle N^+ K^+ | \Lambda \rangle^{(N_f L)} = \left(\frac{1 + \delta_{\Lambda 0} \delta_{K^+ 0}}{1 + \delta_{K^+ 0}} \right)^{1/2} \left(\frac{2N^+ + 1}{2N_f + 1} \right)^{1/2} \langle N_f \Lambda + K^+ | L \Lambda, N^+ K^+ \rangle,$$

which is the usual type of 'rotational frame transformation amplitude' that has entered many other treatments of molecular Rydberg states (Greene & Jungen 1985; Child & Jungen 1990; Fano 1970). That is to say, this amplitude describes the physics of the l-uncoupling which occurs as a Rydberg electron roams farther and farther from the ionic core and eventually 'looks back' and 'sees' the residual ionic core in a specific rotational level $N^+ K^+$. A second projection factor in the full frame transformation matrix is the amplitude for an ion in a specific vibrational level $|v^+ \Gamma^+\rangle^{(N^+ K^+)}$ to have the nuclei at normal coordinate positions $|\boldsymbol{Q}\rangle$ as the Rydberg electron enters the core region ($r < r_0$). This factor is just the ionic vibrational wavefunction $\langle v^+ \Gamma^+ | \boldsymbol{Q} \rangle^{(N^+ K^+)}$.

We turn now to a discussion of some of the more critical symmetry aspects for this system. A crucial element of the present MQDT formulation is the use of a body-frame, nuclear-geometry dependent reaction matrix $K_{\Lambda,\Lambda'}(\boldsymbol{Q})$ which is *non-diagonal* in the electronic projections Λ, Λ'. Staib & Domcke (1990) have discussed the $\Lambda = \pm 1$ form of this body-frame reaction matrix, employing the Longuet–Higgins

(1961) parametrization of the JT Hamiltonian. This body-frame reaction matrix (or JT Hamiltonian) would remain *diagonal* if the nuclei remained constantly in a D_{3h} configuration, because the group symmetry quantum numbers would then be exactly conserved. Earlier diatomic frame transformation studies, in fact, assumed that the body-frame reaction matrix was diagonal (Greene & Jungen 1985; Jungen & Dill 1980; Jungen & Atabek 1977). Our formulation describes non-D_{3h} distortions and all vibrational interactions within each non-degenerate Rydberg series ($\Lambda = \Lambda' = 0$), as well as JT interactions ($\Lambda \neq \Lambda'$) between doubly degenerate Rydberg series and their associated continua. The body-frame matrix has the structure

$$K_{\Lambda,\Lambda'}(\boldsymbol{Q}) = \begin{array}{c} \\ 0 \\ 1 \\ -1 \end{array} \begin{array}{c} \begin{array}{ccc} 0 & 1 & -1 \end{array} \\ \begin{pmatrix} \tan[\pi\mu_{\Lambda=0}(\boldsymbol{Q})] & 0 & 0 \\ 0 & \delta\rho^2 & \lambda\rho\exp[\mathrm{i}\phi] \\ 0 & \lambda\rho\exp[-\mathrm{i}\phi] & \delta\rho^2 \end{pmatrix} \end{array}, \tag{2.2}$$

which includes a key for the values of Λ associated with the appropriate channels. Here ρ, ϕ are the radial and azimuthal coordinates of the doubly degenerate vibrational modes which describe bending vibrations and λ, δ are the Jahn–Teller coupling constants (Staib & Domcke 1990; Longuet-Higgins 1961). The radial and azimuthal coordinates of the doubly degenerate vibrational modes are given in terms of normal coordinates $\boldsymbol{Q}$ and bond stretching coordinates Δr_i ($i = 1, 2, 3$) through the following relations:

$$\rho = (Q_a^2 + Q_b^2)^{1/2}, \tag{2.3}$$

$$Q_a = (\tfrac{2}{3} m_{\mathrm{p}}\omega_0)^{1/2} \frac{1}{\sqrt{6}} (\Delta r_1 + \Delta r_2 - 2\Delta r_3), \tag{2.4}$$

$$Q_b = (\tfrac{2}{3} m_{\mathrm{p}}\omega_0)^{1/2} \frac{1}{\sqrt{2}} (\Delta r_1 - \Delta r_2), \tag{2.5}$$

and the fully symmetric vibrational coordinate is

$$Q_1 = (\tfrac{1}{3} m_{\mathrm{p}}\omega_0)^{1/2} \frac{1}{\sqrt{3}} (\Delta r_1 + \Delta r_2 + \Delta r_3), \tag{2.6}$$

where $\omega_0 = 2521.3\,\mathrm{cm}^{-1}$ is the fundamental vibrational frequency of H_3^+ and m_{p} is the proton mass.

The $\Lambda = \pm 1$ terms in equation (2.2) are derived by expanding matrix elements of the body-frame adiabatic Hamiltonian of a D_{3h} molecule in powers of the normal coordinates (Longuet-Higgins 1961). Equation (2.2) ignores quadratic terms in the off-diagonal elements of the $\Lambda = \pm 1$ submatrix. The constant, zero-order term of this expansion represents the $\Lambda = \Lambda' = \pm 1$ quantum defect which has been omitted from equation (2.2). Denoting this equilibrium quantum defect by $\mu_{e'}^0 = \mu_{\Lambda=\pm 1}(\boldsymbol{Q} = \boldsymbol{0})$, we can include it by using a phase-renormalized base pair $(\tilde{f}_i, \tilde{g}_i)$ of Coulomb wavefunctions (Eissner *et al.* 1969; Giusti-Suzor & Fano 1984). This base pair is given by $\tilde{f}_i = f_i \cos(\pi\mu_{e'}^0) - g_i \sin(\pi\mu_{e'}^0)$ and $\tilde{g}_i = g_i \cos(\pi\mu_{e'}^0) + f_i \sin(\pi\mu_{e'}^0)$, where (f_i, g_i) are the Coulomb wavefunctions defined in equation (2.1). (Alternatively, the quantum defect $\mu_{e'}^0$ can be incorporated by adding a diagonal matrix, equation (2) of Staib & Domcke (1990), to the short-range reaction matrix.) In the $(\tilde{f}_i, \tilde{g}_i)$ basis of Coulomb functions the form of the $\Lambda = \pm 1$ subblock of our K matrix, in matrix notation, is then

$$\boldsymbol{K} = (\tan[\pi\mu_{e'}^0]\boldsymbol{I} + \tilde{\boldsymbol{K}})(\boldsymbol{I} - \tan[\pi\mu_{e'}^0]\tilde{\boldsymbol{K}})^{-1}, \tag{2.7}$$

where $\boldsymbol{I}$ is the unit matrix and $\tilde{\boldsymbol{K}}$ is the $\Lambda = \pm 1$ submatrix in equation (2.2) in the vibrational basis.

The frame transformation in equation (2.2) for matrix elements involving the bending and asymmetric stretch vibrational states ($\Gamma^+ = E'$) uses rovibrational states of the form (Spirko *et al.* 1985)

$$|N^+K^+M^+v^+E'\rangle = \frac{1}{\sqrt{2}}(|N^+K^+M^+E'_b\rangle|v^+E'_a\rangle - |N^+K^+M^+E'_a\rangle|v^+E'_b\rangle). \quad (2.8)$$

These satisfy antisymmetry and total parity requirements and yield a real laboratory frame K matrix. The $|v^+E'_a\rangle$ and $|v^+E'_b\rangle$ are degenerate components of vibrational states with excitation v^+, and $|N^+K^+M^+E'_b\rangle$ and $|N^+K^+M^+E'_a\rangle$ are symmetrized (symmetric top) rotational basis functions:

$$|N^+K^+M^+E'_a\rangle = \frac{1}{\sqrt{2}}(|N^+K^+M^+\rangle + (-1)^{N^++K^+}|N^+ - K^+M^+\rangle), \quad (2.9)$$

$$|N^+K^+M^+E'_b\rangle = \frac{i(-1)^\sigma}{\sqrt{2}}(|N^+K^+M^+\rangle - (-1)^{N^++K^+}|N^+ - K^+M^+\rangle), \quad (2.10)$$

where $\sigma = K^+(\mathrm{mod}\ 3)$, i.e. $\sigma =$ even for $K^+ = 2 + 3t$, $t = 0, 1, 2\ldots$. For the non-degenerate vibrational core states ($\Gamma^+ = A'_1$), the rovibrational basis function is $i|N^+0M^+\rangle|v^+A'_1\rangle$. We have chosen phase conventions for these functions identical to those of Spirko *et al.* (1985). The overall symmetry of the rovibrational levels can be specified by the quantum numbers G, U and s ($K^+ = G - U$, $U = \pm 1$, $s = \pm 1$) (Watson 1984). The total parity is specified by $(-1)^{K^+}$, where levels labelled $'$ have overall even parity and those labelled $''$ have odd parity.

The $\Lambda = \Lambda' = 0$ contributions occurring in equation (2.2) relate to a quantum defect matrix $\mu_{0\Gamma^+v^+,0\Gamma'^+v'^+}$. By initially constructing this matrix instead of the K matrix, we bypass the numerically troublesome integration over possible poles of the function $\tan[\pi\mu_{\Lambda=0}(\boldsymbol{Q})]$ (weighted by products of vibrational wavefunctions). Next we form its eigenvectors $U_{0\Gamma^+v^+,\alpha}$ and eigenvalues μ_α and the K matrix elements needed for the multichannel quantum defect calculation are obtained from

$$K_{0\Gamma^+v^+,0\Gamma^{+\prime}v^{+\prime}} = \sum_\alpha U_{0\Gamma^+v^+,\alpha} \tan[\pi\mu_\alpha](\boldsymbol{U}^{\mathrm{T}})_{\alpha,0\Gamma^{+\prime}v^{+\prime}}. \quad (2.11)$$

The equilibrium value $\mu^0_{a''_2} = \mu_{\Lambda=0}(\boldsymbol{Q} = \boldsymbol{0})$ of the out-of-plane quantum defect function enters our calculation as the leading term in a third-order Taylor expansion of $\mu_{\Lambda=0}(\boldsymbol{Q})$ about $\boldsymbol{Q} = \boldsymbol{0}$.

3. Discussion

In figure 1 we show an energy level diagram in the region of the lowest ionization thresholds of H_3^+. Three regions are also indicated ('open' continuum, Beutler–Fano region and discrete region) where Bordas *et al.* (1991) measured production of H_3^+ ions by photoabsorption from the neutral $1s^2 3s\,{}^2A'_1$, $v_i = 0$, $N_i = 1$, $K_i = 0$ Rydberg state. At particular photon energies neutral Rydberg states attached to rotationally and vibrationally excited ionic core states are populated, which are observed as autoionizing resonances (interlopers) in any region of the photoabsorption spectrum above the first ionization threshold. These resonances decay by rotational and vibrational preionization by energy exchange during close collision of the Rydberg

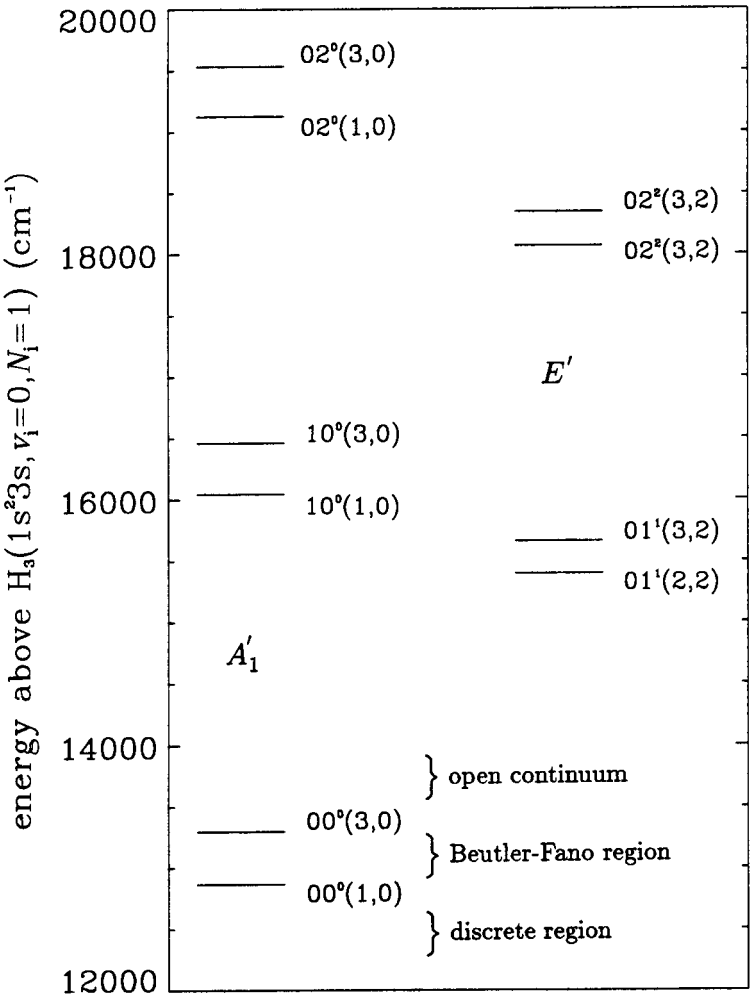

Figure 1. Vibrational energy levels of H_3^+ in the energy range of relevance to the present study. Here ν_1 and ν_2 indicate vibrational quanta in the symmetric and bending modes, ℓ is vibrational angular momentum and N^+, K^+ are the rotational quantum numbers. From Stephens & Greene (1995).

electron with the ion core. Below the first ionization threshold these states cannot autoionize, but instead appear as local perturbations on otherwise normal Rydberg series converging to this threshold.

In figure 2 we show our calculations of the summed ($N_f = 0 + 2$ results) oscillator strength in the energy range above the lowest $(N^+, K^+, \Gamma^+) = (1, 0, 1A_1')$ ionization threshold, compared to the spectrum measured by Bordas *et al.* (1991). The theoretical spectrum has been convolved with a Gaussian detector function with FWHM = 0.15 cm^{-1}. In figure 2 we have labelled resonances a–l according to figure 3 of Bordas *et al.* (1991). Resonances labelled m–p by us are also indicated in figure 2 and in figure 3, which enlarges the Beutler–Fano and near continuum portion of these spectra. The experimental resonances labelled b and c were assigned by Bordas *et al.* (1991) as autoionizing d ($\ell = 2$) Rydberg states, and accordingly our calculation cannot predict these since we presently include only p waves. The

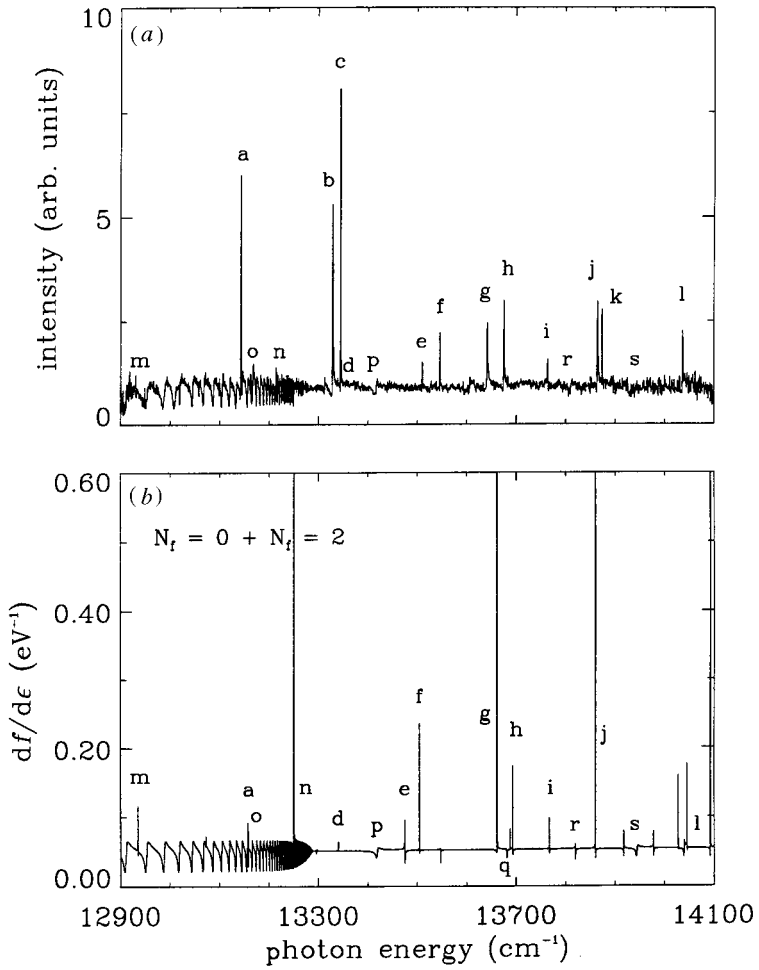

Figure 2. Comparison of theoretical calculations with the experimental results of Bordas *et al.* (1991), for the photoionization of the $1s^2 3s\,^2A_1'$ state of H_3. From Stephens & Greene (1995).

observed resonance a is assigned as due to an interloper state in the $N_f = 2$ branch. The resonance labelled n is stronger and narrower in the theoretical prediction than is seen in the experiment. It is possible that the resonance observed in the experiment is predissociated by coupling to the repulsive ground state, as is the prominent resonance observed in the discrete region near the $(1, 0, 1A_1')$ threshold (discussed below). The resonances labelled o, p, q, r, s and l in figure 2 are members of Rydberg series converging to the lowest ionic core levels $(2, 2, 1E')$ and $(3, 2, 1E')$. For these autoionizing states the Rydberg electron electronic angular momentum projections have $\Lambda = \pm 1$ in Hund's case (b), i.e. those whose electronic degeneracy is lifted by the Jahn–Teller interaction. Due to the rotational ℓ uncoupling in this branch, however, these states also contain some mixing with the $\Lambda = 0$ (a_2'') case (b) states.

Resonances predicted in the $N_f = 0$ final state (see figure 4*a* of Stephens & Greene (1995), or the bottom of figure 5 below) decay solely from vibrational autoionization, via energy exchange with the fully symmetric stretch modes. In figure 2, many resonances in the $N_f = 2$ channel decay solely from *non-vanishing* vibrational K matrix elements of the form $\langle v^+ A_1' | Q_a + \mathrm{i}Q_b | v^{+'} E' \rangle$. This interaction permits the

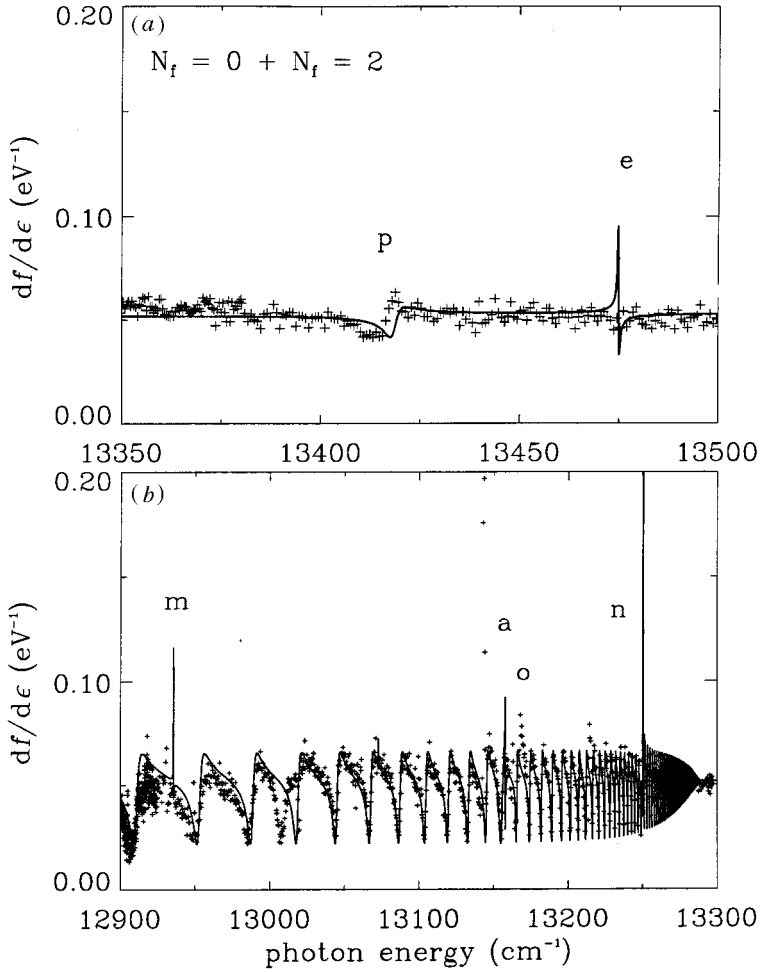

Figure 3. Comparison of theoretical calculations with the experimental results of Bordas *et al.* (1991), for the photoionization of the $1s^2 3s\, ^2A_1'$ state of H_3. Two regions are shown on an expanded scale. The crosses are the (normalized) experimental points of Bordas *et al.* (1991) and the lines are present theory. From Stephens & Greene (1995).

Rydberg states attached to bending modes of the H_3^+ ion to decay into the observed $(N^+, K^+, \Gamma^+) = (1, 0, 1A_1')$ and $(3, 0, 1A_1')$ continua, the strength of which is determined by the magnitude of the off-diagonal matrix elements in equation (2.2). (Here and below, $n\Gamma^+$ indicates a particular vibrational state of symmetry Γ^+, $n = 1$ being the lowest in energy.) Inclusion of this Jahn–Teller coupling mechanism allows scattering of the Rydberg electron between the $\Lambda = 1$ and $\Lambda = -1$ components at short range in the e^-–H_3^+ complex and is essential to account for many of the resonances observed by Bordas *et al.* (1991).

In figure 3 we show on an enlarged scale a comparison of theory and experiment in the continuum region (top) of the p resonance and the Beutler–Fano region (bottom) which extends from 12 867.6 to 13 297.5 cm^{-1}. In this figure the experiment was normalized to theory at the single photon energy 13 400 cm^{-1}. The breadth, depth and position of resonance p (and other members of this series) are in reasonable agreement with experiment. These resonances consist of relatively high principal

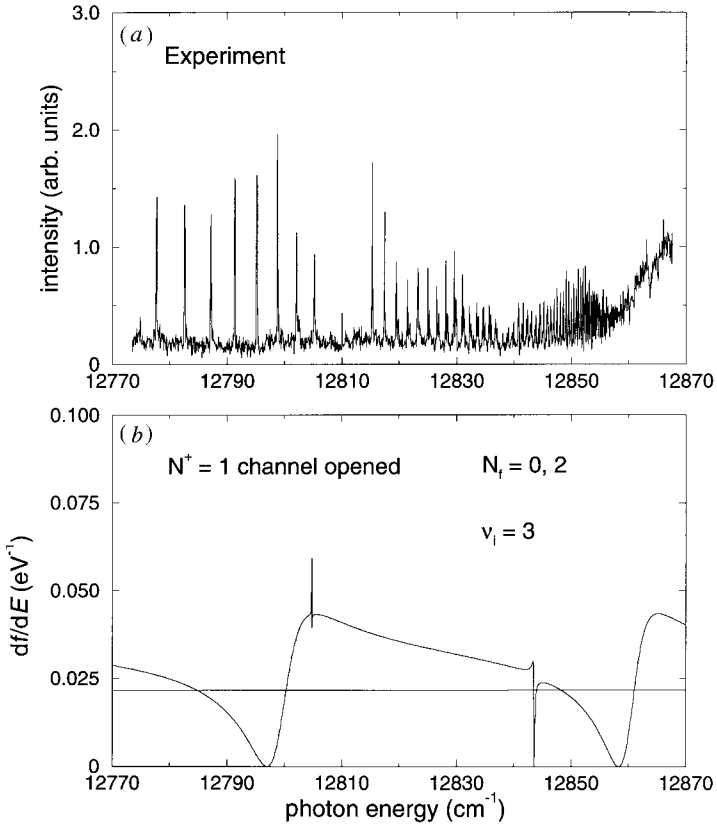

Figure 4. Comparison of theoretical calculations (b) with the experimental results (a) of Bordas *et al.* (1991), for the discrete photoabsorption oscillator strengths excited from the $1s^2 3s\,^2A_1'$ state of H_3. In (b), $N_f = 0$ is shown as a dashed curve, while $N_f = 2$ is shown as a solid curve. Using MQDT we convert the discrete spectrum into a continuous distribution (b) in order to aid in the analysis.

quantum number perturbers ($n \sim 7, 8$) with substantial mixing occurring between closed-channel states attached to the $(2, 2, 1E')$ and $(3, 2, 1E')$ thresholds. In the absence of Jahn–Teller interactions, resonance p would have zero autoionization width, i.e. be a true bound state. In the Beutler–Fano region, figure 3*b*, the excellent fit of the rotational autoionization profiles to experiment relys on incorporating *ab initio* dipole matrix elements for the $3s \rightarrow np_z$ and $3s \rightarrow np_{x,y}$. We also predict perturbers having both $N_f = 0$ (resonance m) and 2 (resonances a, o and n) final state angular momentum, which appear to be partly resolved in the experiment, although additional theoretical and experimental studies are clearly needed to fully characterize them.

In figure 4 we show a plot of our calculated oscillator strength below the first ionization threshold of H_3^+ and the experimental results of Bordas *et al.* (1991) in the same region. Discretization of the continuous oscillator strength for the $N_f = 0$ and $N_f = 2$ final states leads to two Rydberg series converging to the first threshold. This procedure has been discussed by Stephens & Greene (1995) (figure 9 of that paper shows this discretization). Briefly, the two features at 12 810 and 12 860 cm^{-1} can be attributed to the same series of rotationally autoionizing interlopers, which dominate photoionization in the Beutler–Fano region, and which converge to the

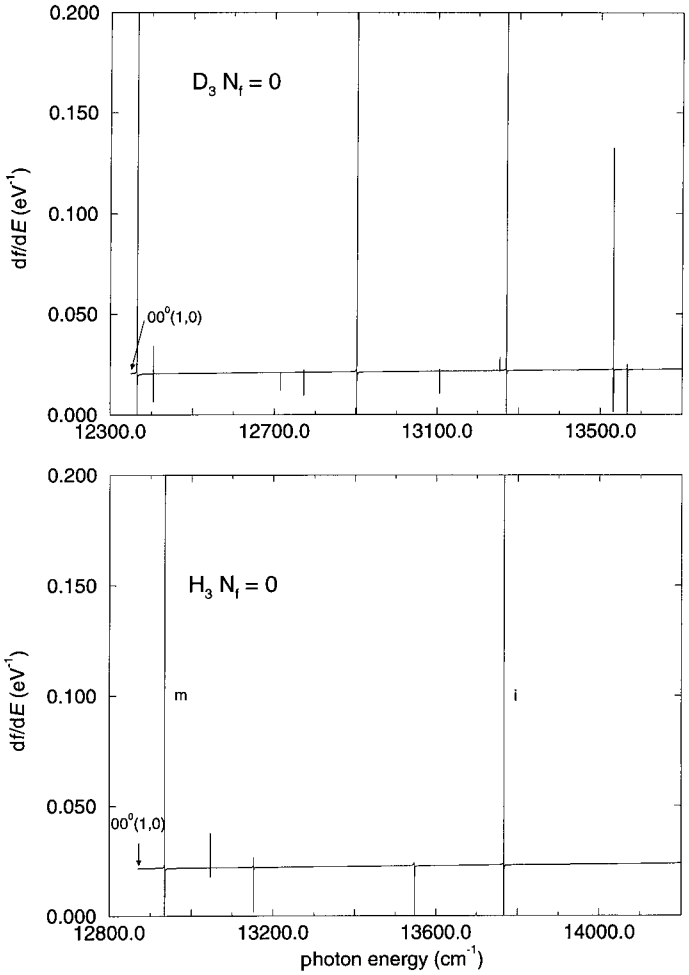

Figure 5. Comparison of our theoretical photoionization spectra of D_3 (preliminary, top) with those for H_3. These final states with total angular momentum $N_f = 0$ are excited from the $1s^2 3s\, ^2A_1'$ states of H_3 and D_3, respectively.

$(3, 0, 1A_1')$ ionic threshold. Our calculation (figure 4*b*) predicts minima for these two interlopers to occur at 12 797 and 12 858 cm^{-1}, respectively. The weak Rydberg series discernible between 12 815 and 12 850 cm^{-1} in figure 4*a* corresponds to the the $N_f = 0$ final state. Accordingly, discretization of the oscillator strength in figure 4*b* leads to a Rydberg series which decreases in intensity as *ca.* n^{-3}. The prominent experimental window feature near 12840 cm^{-1} was attributed by Bordas *et al.* (1991) to a low-n perturber which predissociates due to its coupling with the repulsive $\tilde{X}\ 1s^2 2p\, ^2E'$ ground state of H_3. The calculation in figure 4 is an enlarged MQDT calculation using 52 rovibronic channels, which allows a low-n ($n \sim 3$) perturber to appear within *ca.* 100–150 cm^{-1} of the broad feature near 12 840 cm^{-1}. This is seen near 12 843 cm^{-1} in figure 4*b*. As in H_2, the low-n states of H_3 in this energy range have a large vibrational energy, and hence can predissociate rapidly. Our enlarged MQDT calculation, despite the assumption of energy independence of the quantum defect, nonetheless lends some support to this assignment. To fully account for this feature,

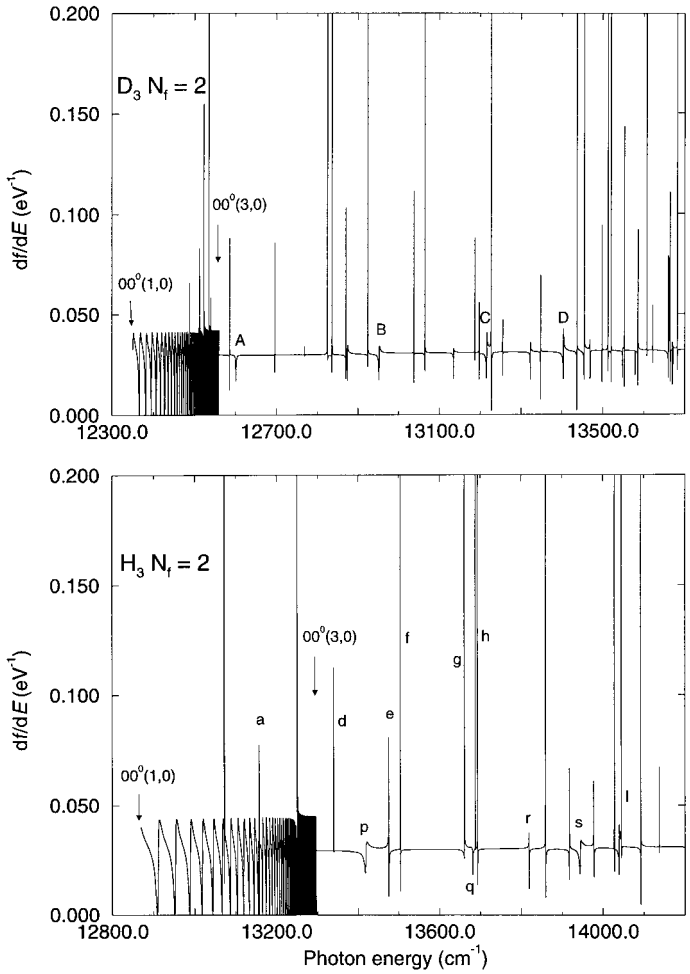

Figure 6. Comparison of our theoretical photoionization spectra of D_3 (preliminary, top) with those for H_3. These final states with total angular momentum $N_f = 2$ are excited from the $1s^2 3s\,{}^2A_1'$ states of H_3 and D_3, respectively.

the present theory needs to be extended to incorporate predissociation within a unified MQDT framework (Jungen 1984; Gao *et al.* 1993).

In figures 5 and 6 we show calculations for photoionization of the $1s^2 3s\,{}^2A_1'$, $v_i = 0$, $N_i = 1$, $K_i = 0$ Rydberg state of D_3 for total final state angular momenta $N_f = 0$ and 2. The ionization thresholds are labelled using the notation of figure 1 and the autoionizing resonances for H_3 are labelled as discussed previously. In the bottom half of these figures we compare the D_3 results with their H_3 counterparts. These calculations span a spectral region of *ca.* 1400 cm^{-1} above the $v^+ = 0$, $N^+ = 1$, $K^+ = 0$ ionic threshold. For D_3 we have used the JT coupling constants $\lambda = 11\,535\ cm^{-1}$, $\delta = 433\ cm^{-1}$ and the fundamental vibrational frequency of $\omega_0 = 1834.7\ cm^{-1}$ (Watson *et al.* 1987). To obtain the JT constants for D_3, we used the relations $\lambda_{D_3} = R^{1/2}\lambda_{H_3}$ and $\delta_{D_3} = R\delta_{H_3}$, where

$$R = m_p \omega_0^{H_3^+} / m_d \omega_0^{D_3^+}.$$

(These follow from equations (2.4) and (2.5) and the definition of the JT coupling con-

stant in terms of the body-frame Rydberg eigenvalue ϵ, $\lambda = -\partial\epsilon/\partial Q_a = -\partial\epsilon/\partial Q_b$. An analogous relation for δ holds for second derivatives.) We determined the ionization potential of the $1s^2 3s\,{}^2A_1'$, $v_i = 0$, $N_i = 1$, $K_i = 0$ Rydberg state relative to the $v^+ = 0$, $N^+ = 1$, $K^+ = 0$ ionic threshold to be 12 343 cm^{-1}. This ionization potential was calculated from a combination of available data (Dabrowski & Herzberg 1980; Figger *et al.* 1984, 1989; Ketterle *et al.* 1989). (Owing to imprecise data for the 3p-to-threshold term value (Figger *et al.* 1984), our ionization potential may be in error by as large as *ca.* 100–500 cm^{-1}.) We used the same number of ionic channels (40 total) in the MQDT calculation as in our previous calculations on H_3 (Stephens & Greene 1995) and each spectrum contains 10^5 points over the indicated spectral range.

Examining figures 5 and 6, it is clear that in proceeding from H_3 to the species D_3, no simple modification of the spectrum is apparent, particularly in terms of resonance positions and patterns. This is due to the different rotational structure of the ion (the vibrational ground-state rotational spacings are 217 cm^{-1} and 430 cm^{-1} for D_3^+ and H_3^+, respectively) and the isotopic (nuclear mass) dependence of the Jahn–Teller coupling constants λ, δ. The most striking differences are the appearance of more autoionizing resonances in the case of D_3, due to the higher density of vibrational ionic states, and the narrowing of autoionizing resonances in the $N_f = 2$ final state, due to the weaker Jahn–Teller coupling in this heavier molecule. The narrowing of resonances is most apparent for Rydberg states converging to the first or second bending vibrational mode of the ion. For example, resonances of this type in D_3 are predicted in figure 6 to occur near 12 600, 12 950, 13 210 and 13 400 cm^{-1}, labelled 'A–D' in the top of figure 6. Their widths are predicted to be substantially smaller than the analogous type of H_3 resonances. These resonances are labelled 'p', 'q', 'r' and 's' in the bottom of figure 6 and have been discussed previously (Stephens & Greene 1995).

One simplifying aspect in the spectrum of D_3 compared to H_3 should be the weakening (or disappearance) of prominent features due to predissociation of low-n perturbers, such as the example discussed above for H_3. This possibility was pointed out in the model calculations of H_3 and D_3 by Staib & Domcke (1990). This effect has already been clearly observed in emission spectra proceeding from H_3 to all deuterated species, particularly in D_3 for emission near the wavelength 7100 Å (Figger *et al.* 1989; Ketterle *et al.* 1989).

It remains of interest to perform a detailed investigation of the Jahn–Teller coupling mechanism in the D_3 Rydberg states discussed above, and also to examine the importance of predissociation in the Rydberg states of D_3.

Work at the University of Colorado was supported by the National Science Foundation.

References

Bordas, M. C. & Helm, H. 1991 Predissociation of H_3 near its ionization threshold induced by very weak electric fields. *Phys. Rev.* A **43**, 3645–3651.

Bordas, M. C., Lembo L. J, & Helm, H. 1991 Spectroscopy and multichannel quantum-defect theory analysis of the *np* Rydberg series of H_3. *Phys. Rev.* A **44**, 1817–1827.

Child, M. S. & Jungen, Ch. 1990 Quantum defect theory for asymmetric tops: application to the Rydberg spectrum of H_2O. *J. Chem. Phys.* **93**, 7756–7766.

Dabrowski, I. & Herzberg, G. 1980 The electronic emission spectrum of triatomic hydrogen. I. Parallel bands of H_3 and D_3 near 5600 and 6025 Å. *Can. J. Phys.* **58**, 1238–1249.

Eissner, W., Nussbaumer, H., Saraph, H. E. & Seaton, M. J. 1969 Resonances in cross sections for excitation of forbidden lines in O^{2+}. *J. Phys.* B **2**, 341–355.

Fano, U. 1970 Quantum defect theory of ℓ uncoupling in H_2 as an example of channel-interaction treatment. *Phys. Rev.* A **2**, 353–365.

Figger, H., Fukuda, Y., Ketterle, W. & Walther, H. 1984 Spectra and lifetimes of triatomic hydrogen molecules. *Can. J. Phys.* **62**, 1274–1279.

Figger, H., Ketterle, W. & Walther, H. 1989 Spectroscopy of triatomic hydrogen. I. Bands near 5600, 5800 and 6025 Å. *Z. Phys.* D **13**, 129–137.

Gao, H., Jungen, Ch. & Greene, C. H. 1993 Predissociation of H_2 in the $3p\pi D\ ^1\Pi_u^+$ state. *Phys. Rev.* A **47**, 4877–4884.

Giusti-Suzor, A. & Fano, U. 1984 Alternative parameters of channel interactions. I. Symmetry analysis of the two-channel coupling. *J. Phys.* B **17**, 215–230.

Greene, C. H. & Jungen, Ch. 1985 Molecular applications of quantum defect theory. *Adv. At. Mol. Phys.* **21**, 51–121.

Helm, H. 1986 Observation of high-n Rydberg series ($7 < n < 40$) of the H_3 molecule. *Phys. Rev. Lett.* **56**, 42–45.

Jungen, Ch. 1984 Unified treatment of dissociation and ionization processes in molecular hydrogen. *Phys. Rev. Lett.* **53**, 2394–2397.

Jungen, Ch. & Atabek, O. 1977 Rovibronic interactions in the photoabsorption spectrum of molecular hydrogen and deuterium: an application of multichannel quantum defect methods. *J. Chem. Phys.* **66**, 5584–5609.

Jungen, Ch. & Dill, D. 1980 Calculation of rotational–vibrational preionization in H_2 by multichannel quantum defect theory. *J. Chem. Phys.* **73**, 3338–3345.

Ketterle, W., Figger, H. & Walther, H. 1989 Spectroscopy of triatomic hydrogen. II. Bands near 4500 and 7100 Å. *Z. Phys.* D **13**, 139–146.

Lembo, L. J., Helm, H. & Huestis, D. L. 1989 Measurement of vibrational frequencies of the H_3 molecule using two-step photoionization. *J. Chem. Phys.* **90**, 5299–5308.

Longuet-Higgins, H. C. 1961 Some recent developments in the theory of molecular energy levels. In *Advances in spectroscopy*, vol. II, pp. 429–474. New York: Interscience.

Nager, Ch. & Jungen, M. 1982 Potential surfaces for the Rydberg states of H_3. *Chem. Phys.* **70**, 189–198.

Pan, S. & Lu, K. T. 1988 Triatomic molecular H_3 frame transformation theory of the ℓ-uncoupling effect. *Phys. Rev.* A **37**, 299–302.

Seaton, M. J. 1983 Quantum defect theory. *Rep. Prog. Phys.* **46**, 167–257.

Sobolewski, A. L. & Domcke, W. 1988 Resonances in molecular photoionization. III. Multichannel extension and application to polyatomic molecules. *J. Chem. Phys.* **88**, 5571–5579.

Spirko, V., Jensen, P., Bunker, P. R. & Cejchan, A. 1985 The development of a new Morse-oscillator based rotation–vibration Hamiltonian for H_3^+. *J. Mol. Spectrosc.* **112**, 183–202.

Staib, A. & Domcke, W. 1990 Analysis of the Jahn–Teller effect in the $np\ ^2E'$ Rydberg series of H_3 and D_3. *Z. Phys.* D **16**, 275–282.

Staib, A., Domcke, W. & Sobolewski, A. L. 1990 Jahn–Teller effect in Rydberg series: a multistate vibronic coupling problem. *Z. Phys.* D **16**, 49–60.

Stephens, J. A. & Greene, C. H. 1994 Quantum defect description of H_3 Rydberg state dynamics. *Phys. Rev. Lett.* **72**, 1624–1627.

Stephens, J. A. & Greene, C. H. 1995 Rydberg state dynamics of rotating, vibrating H_3 and the Jahn–Teller effect. *J. Chem. Phys.* **102**, 1579–1591.

Watson, J. K. G. 1984 Higher-order vibration–rotation energies of the X_3 molecule. *J. Mol. Spec.* **103**, 350–363.

Watson, J. K. G., Foster, S. C., & McKellar, A. R. W. 1987 The infrared spectrum of the ν_2 fundamental band of the D_3^+ molecular ion. *Can. J. Phys.* **65** 38–46.

PHILOSOPHICAL TRANSACTIONS OF THE ROYAL SOCIETY A MATHEMATICAL, PHYSICAL & ENGINEERING SCIENCES